Journal of the Australian Ceramic Society (2020) 56:79–90
https://doi.org/10.1007/s41779-019-00386-8

RESEARCH

A thermodynamic study on $PbZr_{0.52}Ti_{0.48}O_3$ ceramic close to the tetragonal-cubic transition

Ali Kiraci[1]

Received: 8 June 2018 / Revised: 29 May 2019 / Accepted: 21 June 2019 / Published online: 25 July 2019

Abstract

The isobaric Grüneisen parameter and the wavenumber (frequency) of various Raman modes in $PbZr_{1-x}Ti_xO_3$ (PZT x = 0.48) ceramic were calculated by means of the unit cell volume of this crystal. In addition, the damping constant (linewidth) of the Raman modes studied was computed from the pseudospin-phonon coupled and from the energy fluctuation models close to the tetragonal-cubic transition temperature of $T_C = 650$ K. This calculation of the damping constant performed in terms of the order parameter (spontaneous polarization), which was associated with the wavenumbers of the Raman modes studied. Furthermore, the inverse relaxation time of the Raman modes in this ceramic calculated and the values of the activation energy were deduced in terms of the Arrhenius plot close to the tetragonal-cubic transition in PZT ($x = 0.48$) ceramic. Finally, the temperature dependence of some thermodynamic quantities, such as the isothermal compressibility and the specific heat of this ceramic, was predicted.

Keywords PZT ($x = 0.48$) · Grüneisen parameter · Wavenumber · Damping constant · Specific heat

Introduction

Lead zirconate titanate, $PbZr_{1-x}Ti_xO_3$ (PZT), has been the subject of both experimental and theoretical studies due to its potential applications in industry such as transducers and ultrasonic motors [1, 2]. Those studies have been particularly focused across the morphotropic phase boundary (MPB) around $x = 0.48$, due to the fact that the highest piezoelectric and electromechanical coupling coefficients of PZT ceramics have been observed at this composition of $x = 0.48$ [3]. MPB was considered as the region between the ferroelectric rhombohedral and tetragonal phases as a coexistence phase [3]. The low-temperature rhombohedral phase, $F_{R(LT)}$, with a symmetry group of R3c and the high-temperature rhombohedral phase, $F_{R(HT)}$, with a symmetry group of R3m have been reported in PZT ceramic by Michel et al. [4] in relation to the different tilt of the oxygen octahedra, as also pointed out previously [5]. This tilting of the oxygen octahedra in the $F_{R(LT)}$ phase doubles the unit cell volume when compared with the $F_{R(HT)}$ phase [6]. It is also reported that below $F_{R(LT)}$, PZT is in the antiferroelectric orthorhombic phase with a space group Pba2, while it is in the cubic paraelectric phase with a space group Pm3m above the $F_{R(HT)}$ phase [7].

Although various experimental techniques have carried out near the MPB of PZT ceramics, the boundaries between the different phases have not understood totally, yet. The composition (x)-temperature (T) phase diagram of PZT compounds near the MPB has been reported by Kim et al. [8], Bouzid et al. [9], Eitel and Randall [10], and Buixaderas et al. [11]. Also, the pressure (P)-temperature (T) phase diagram of PZT ($x = 0.48$) has been studied by Rouquette et al. [12] and Audigier et al. [13]. In addition, the static compression data (volume-pressure relation) for PZT ($x = 0.48$) ceramic has been reported by Cho et al. [14]. In their high-resolution synchrotron x-ray powder diffraction experiment, Noheda et al. [15] have reported the temperature dependence of the lattice parameters of the PZT crystal with $x = 0.48$ up to the 700 K. Phelan et al. [16], Hlinka et al. [17], Gorfman et al. [18], and Bokov et al. [19] have studied the structural, electrical, and optical properties of PZT single crystals close to the MPB. In their Raman spectroscopy experiment, Filho et al. [20] have showed the stability of the monoclinic phase in a narrow region close to the MPB in PZT ($x = 0.48$) ceramic by using the Landau-Devonshire phenomenological theory.

Shifting of the atoms from their ideal positions makes it very difficult to explain the phase transition mechanism of

✉ Ali Kiraci
akiraci@cankaya.edu.tr

[1] Inter-Curricular Courses Department, Cankaya University, Ankara, Turkey

PZT ceramics [21]. Especially, off-center Pb displacements pointed out the existence of an intrinsic short range dynamic disorder over the PZT compound, as also pointed out previously [22–26]. The infrared active modes of lead-based perovskites (ABO_3, where A = Pb), vibrating along the mode dipole moment, are divided into three parts namely, Last, Slater, and Axe bands, according to the character of the eigenvectors (vibrations) [27]: eigenvectors related to the Pb-cations against BO_6 octahedra appear below 150 cm^{-1} (Last band); vibrations related to the B atom against the O_6 octahedra appear between 200 and 450 cm^{-1} (Slater band) and those related to the bending of the O_6 octahedra appear above 500 cm^{-1} (Axe band). The A_1(TO1) and E(TO1) Raman modes are the examples of the Last band, while the A_1(TO2), B_1, and E(TO2) mode examples of Slater band similarly, the A_1(TO3) and E(TO3) mode examples of the Axe band. Recently, we have calculated some thermodynamic quantities such as damping constant and the relaxation time of the longitudinal acoustic (LA) mode, close to the ferroelectric-paraelectric phase transition temperature of $T_C = 657$ K in PZT (x = 0. 45) [28].

In this study, the unit cell volume of the PZT ($x = 0.48$) crystal has been calculated as a function of temperature in terms of the lattice parameters of the solid solution of PZT ($x = 0.48$) reported in the literature [15]. The isobaric mode Grüniesen parameter and the wavenumber of the A_1(TO1), A_1(TO2), B_1, E(TO1), and E(TO2) Raman modes in PZT ($x = 0.48$) ceramic were then calculated by using the estimated values of the unit cell volume of the PZT ($x = 0.48$) crystal. Those calculated values of the wavenumber were then associated with the order parameter to evaluate the damping constant of the Raman modes, indicated above from the pseudospin-phonon coupled and the energy fluctuation models. The inverse relaxation time and the values of the activation energy of the Raman modes in PZT ($x = 0.48$) were also computed. Lastly, the specific heat and the isothermal compressibility of this PZT ceramic were evaluated by using the P-T relation of this compound from the literature.

Below, in section "Theory", the "theory" part was given. The "calculations and results" and "discussion" parts were given in sections "Calculations and Results" and "Discussion", respectively. Finally, the "conclusions" part was given in section "Conclusions".

Theory

Grüneisen parameter

The anharmonicity of a crystalline system is defined microscopically as Grüneisen parameter γ given by [29, 30]

$$\gamma = -\frac{\partial ln\omega}{\partial \ln V}, \tag{2.1.1}$$

where γ is the dimensionless quantity, ω is the vibrational frequency of the lattice modes, and V is the volume of the crystal. The isobaric Grüniesen parameter $\gamma_p(T)$ can be expressed as

$$\gamma_P(T) = -\frac{V(T)}{\omega(T)}\frac{(\partial\omega/\partial T)_P}{(\partial V/\partial T)_P}. \tag{2.1.2}$$

At constant pressure, the temperature dependence of the frequency $\omega_P(T)$ can be obtained from the integration of the Eq. (2.1.2) as

$$\omega_P(T) = \omega_1 \exp\left[-\gamma_P(\mathrm{T})\ln\left(\frac{V_P(T)}{V_1}\right)\right], \tag{2.1.3}$$

where V_1 and ω_1 in Eq. (2.1.3) are the volume of the crystal and the frequency, respectively, at ambient conditions of T = 0 K and P = 0 Pa.

Damping constant

Yamada et al. [31] developed a model to investigate the damping constant as a function of temperature, due to the interaction between pseudospin and a phonon for NH_4Br. Matsushita [32] extended this model by considering the interaction between a pseudospin and two phonons. In their study, Laulicht and Luknar [33] expressed the dynamic scattering function of the pseudospins $S\left[\overrightarrow{q}, \omega \approx 0\right]$ in terms of the damping constant $\Gamma(k_\upsilon, \omega_\upsilon)$ of the υ^{th} phonon with wave vector $\overrightarrow{k}$ and the peak frequency ω_υ for KDP as

$$\Gamma(k_\upsilon, \omega_\upsilon) \approx A \int \mathrm{S}\left(\overrightarrow{q}, 0\right) dq, \tag{2.2.1}$$

here, q is the pseudospin wave vector, A is the weakly temperature-dependent constant and the integration should be taken over the Brillouin zone. Laulicht [34] has related the dynamic scattering function $S\left(\overrightarrow{q}, \omega \approx 0\right)$ to the dielectric susceptibility $\chi(q, 0)$, which is also in relation to the spontaneous polarization (order parameter) y as

$$S\left(\overrightarrow{q}, \omega \approx 0\right) \propto \chi(q, 0) \propto 1 - y^2. \tag{2.2.2}$$

Lahajnar et al. [35] have calculated the integration of Eq. (2.2.1), over all q in the Brillouin zone by using the Eq. (2.2.2) and by considering that the damping constant Γ is inversely proportional to the spin-lattice relaxation time T_1 given as

$$\Gamma \propto \frac{1}{T_1} = k_B t\left(1 - y^2\right) \ln\left[\frac{T_C}{T - T_C(1 - y^2)}\right], \tag{2.2.3}$$

where t is the flipping time of the polarization, k_B is the Boltzmann constant, T is the temperature, and T_C is the transition temperature. The damping constant as a function of temperature for the pseudospin-phonon coupled model (Eq. 2.2.3) can be written in the form

$$\Gamma_{sp} = \Gamma_o' + A'\left(1-y^2\right)\ln\left[\frac{T_C}{T-T_C(1-y^2)}\right], \tag{2.2.4}$$

where Γ_o' is the background damping constant (linewidth) and A' is the amplitude with appropriate units.

The temperature dependence of the damping constant due to the pseudospin-phonon coupling can also be calculated by considering the shifting of the phonon frequency, which is the energy fluctuation of the phonon mode with the wave vector k = 0, as reported by Laulicht [34]. In their work, Schaak and Winterfelt [36] have reported another simple expression for the damping constant due to the phonon frequency shift given as

$$\Gamma_{sp}{}^2 \propto \frac{T(1-y^2)}{T-T_C(1-y^2)}. \tag{2.2.5}$$

The energy fluctuation model (Eq. 2.2.5) can then be written as

$$\Gamma_{sp} = \Gamma_o + A\left[\frac{T(1-y^2)}{T-T_C(1-y^2)}\right]^{\frac{1}{2}}, \tag{2.2.6}$$

where Γ_o and A of the energy fluctuation model (Eq. 2.2.6) are the background damping constant and the amplitude, respectively, as before.

The pseudospin-phonon (Eq. 2.2.4) and the energy fluctuation (Eq. 2.2.6) models can be used to extract the values of the activation energy U, using the following expression [37–39]

$$\Gamma_{sp} \cong \Gamma_{vib} + C\exp(-U/k_BT), \tag{2.2.7}$$

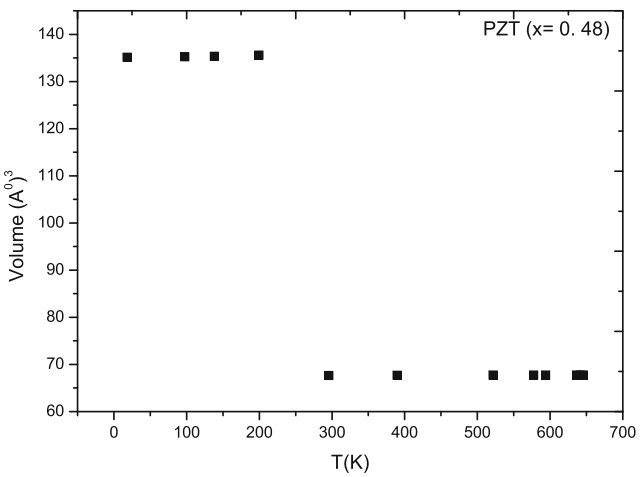

Fig. 1 The unit cell volume of PZT ($x = 0.48$) calculated in terms of the lattice parameters [14] for monoclinic and tetragonal phases

Table 1 Values of the fitting parameters of Eq. (3.1) for the unit cell volume of PZT ($x = 0.48$) within the temperature interval indicated

Ceramic	d_0(Å^3)	d_1x10^{-3}(Å$^3/K$)	Temperature intervals (K)
PZT ($x = 0.48$)	135.0	25.0	18.1 < T < 199.6
	67.6	0.2	295.7 < T < 645.7

in Eq. (2.2.7), C is the constant and k_B is the Boltzmann constant, as before. The vibrational damping constant Γ_{vib} is nearly zero as the transition temperature T_C is approached, as pointed out previously [39]. By taking the natural logarithm of Eq. (2.2.7) with $\Gamma_{vib} = 0$, one can deduced the values of the activation energy U from the slope of the Arrhenious plot $\ln\Gamma_{sp}$ against $1/T$ according to

$$\ln\Gamma_{sp} = \ln C - \frac{U}{k_BT}. \tag{2.2.8}$$

The inverse relaxation time τ^{-1} for the phonon modes of the crystalline systems can be computed from the temperature dependence of the frequency (ω) and the damping constant (Γ) of the relavent phonon modes according to

$$\tau^{-1} = \frac{\omega^2}{\Gamma}. \tag{2.2.9}$$

The cubic (three-phonon process) and quartic (four-phonon process) anharmonicity in lattice vibrations can also be investigated in terms of the frequency and the damping constant of the Raman modes according to the relations read as [40, 41]

Table 2 Values of the fitting parameters of Eq. (3.2) for the Raman modes in PZT ($x = 0.48$) ceramic within the temperature interval indicated

Raman mode	e_0 (cm^{-1})	e_1x10^{-2} (cm^{-1}/K)	e_2x10^{-5} (cm^{-1}/K^2)	Temperature intervals (K)
A_1(TO1)	159.8	2.4	− 27.5	0 < T < 200.0
	231.7	− 48.5	62.2	200.0 < T < 400.0
	63.0	31.9	− 36.3	400.0 < T < 650.0
A_1(TO2)	340.6	4.2	− 18.0	0 < T < 200.0
	364.0	− 11.9	8.1	200.0 < T < 400.0
	330.3	4.1	− 11.5	400.0 < T < 650.0
B_1	270.3	− 4.8	21.8	0 < T < 200.0
	233.4	26.7	− 47.9	200.0 < T < 400.0
	293.3	− 5.3	1.5	400.0 < T < 650.0
E(TO1)	79.6	− 6.3	4.6	0 < T < 200.0
	112.1	− 27.2	31.4	200.0 < T < 400.0
	28.1	15.7	− 22.8	400.0 < T < 650.0
E(TO2)	205.8	1.1	− 16.4	0 < T < 200.0
	196.9	3.7	− 9.3	200.0 < T < 400.0
	166.0	15.5	− 15.8	400.0 < T < 650.0

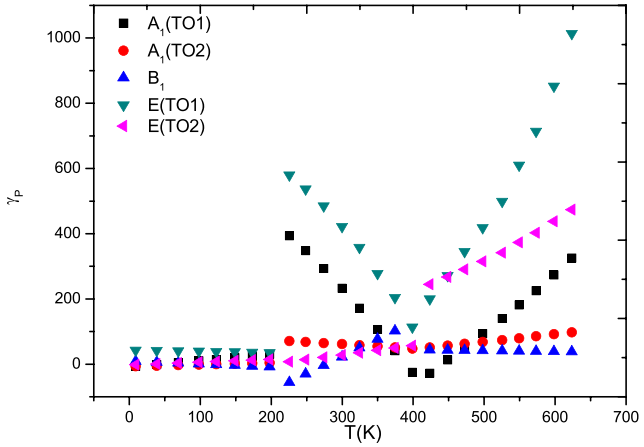

Fig. 2 The isobaric Grüneisen parameter $\gamma_P(T)$ of the A_1(TO1), A_1(TO2), B_1, E(TO1), and E(TO2) Raman modes in PZT ($x = 0.48$) ceramic calculated as a function temperature according to Eq. (2.1.2)

$$\Gamma(T) = \Gamma(0) + A\left(1 + \frac{2}{e^{\frac{a}{T}}-1}\right) + B\left(1 + \frac{3}{e^{\frac{2a}{3T}}-1} + \frac{3}{\left(e^{\frac{2a}{3T}}-1\right)^2}\right) \quad (2.2.10)$$

and

$$\omega(T) = \omega(0) + C\left(1 + \frac{2}{e^{\frac{a}{T}}-1}\right) + D\left(1 + \frac{3}{e^{\frac{2a}{3T}}-1} + \frac{3}{\left(e^{\frac{2a}{3T}}-1\right)^2}\right), \quad (2.2.11)$$

where $\Gamma(0)$ and $\omega(0)$ are the damping constant and the frequency at zero temperature. Also, A, B, C, and D that appear in Eqs. (2.2.10) and (2.2.11) are the constants with appropriate unit of cm^{-1}, and $a = \hbar\omega_0/k_B$ is another constant with a unit of temperature (K). $\hbar$, k_B, and ω_0 are the Planck constant, the Boltzmann constant, and the characteristic frequency of the relevant mode, respectively.

Thermal expansion, isothermal compressibility, and the specific heat

The thermal expansion α_P of a material is defined in terms of its volume V and its temperature derivative at constant pressure as

$$\alpha_P = \frac{1}{V}\left(\frac{\partial V}{\partial T}\right)_P. \quad (2.3.1)$$

The isothermal compressibility κ_T of a material can be evaluated according to the well-known thermodynamic equation

$$\kappa_T = \frac{\alpha_P}{\left(\frac{dP}{dT}\right)}, \quad (2.3.2)$$

where $\frac{dP}{dT}$ is the slope of the pressure-temperature phase diagram of the relevant material.

Also, the difference of the specific heat at constant pressure C_P and the specific heat at constant volume C_V of a material can be calculated using the thermodynamic relation as follows,

$$C_P - C_V = TV\left(\frac{dP}{dT}\right)^2 \kappa_T. \quad (2.3.3)$$

Table 3 Values of the fitting parameters of Eq. (3.3) for the Raman modes in PZT ($x = 0.48$) ceramic within the temperature interval indicated

Raman mode	ω_{max} (cm^{-1})	$f_0 x10^2$ (cm^{-1})	f_1	$f_2 x10^{-3}$ (cm)	Temperature intervals (K)
A_1(TO1)	161.0	6.1	−6.3	21.9	0 < T < 200.0
		4.9	−3.2	7.4	200.0 < T < 400.0
		0.8	1.6	−12.3	400.0 < T < 650.0
A_1(TO2)	344.1	−222.2	133.3	−197.0	0 < T < 200.0
		−58.0	33.8	−46.5	200.0 < T < 400.0
		2.4	0.1	0.5	400.0 < T < 650.0
B_1	273.6	43.0	−29.6	54.3	0 < T < 200.0
		−0.9	3.1	−6.8	200.0 < T < 400.0
		−33.0	24.7	−42.5	400.0 < T < 650.0
E(TO1)	78.7	−2.1	6.7	−37.3	0 < T < 200.0
		2.4	−4.1	22.4	200.0 < T < 400.0
		0.32	1.9	−40.9	400.0 < T < 650.0
E(TO2)	205.9	−8.0	9.6	−22.8	0 < T < 200.0
		−0.7	2.6	−6.1	200.0 < T < 400.0
		1.9	0.4	−2.0	400.0 < T < 650.0

The maximum values of the wavenumber for the Raman modes are also given

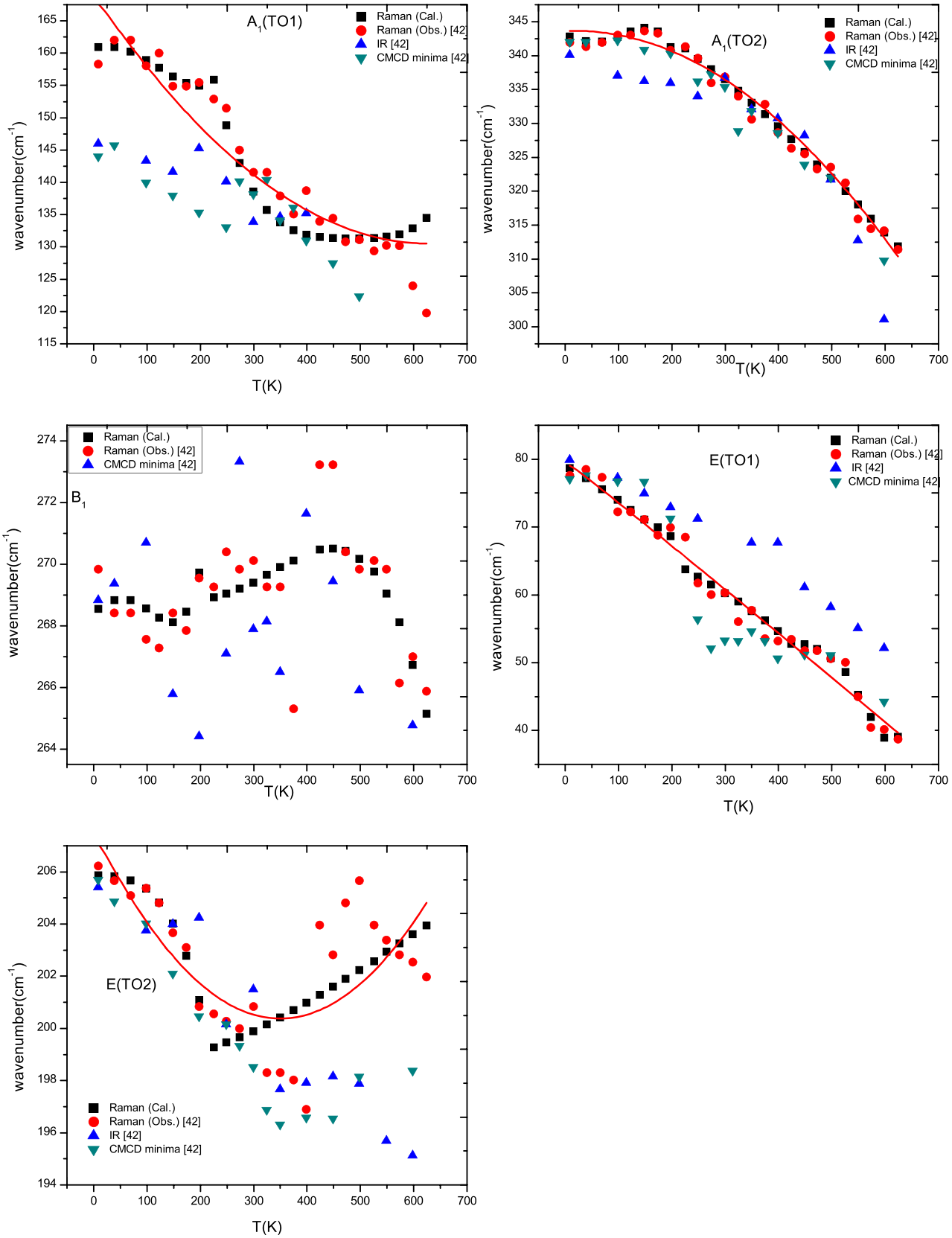

Fig. 3 The calculated values of the wavenumber ω for the Raman modes of A_1(TO1), A_1(TO2), B_1, E(TO1), and E(TO2) in PZT ($x = 0.48$) ceramic according to Eq. (2.1.3). The observed [42] Raman, infrared (IR), and CMCD minima data [42] are also shown for comparison. The red lines show best fit of Eq. (2.2.11) for the observed [42] wavenumber data of these modes

Table 4 Values of the background damping constant Γ_o' (Γ_0) and the amplitudes A'(A) according to the models within the temperature interval indicated for the Raman modes in PZT ($x = 0.48$) ceramic

PZT ($x = 0.48$)	Pseudospin-phonon coupled model (Eq.2.2.4)		Energy fluctuation model (Eq. 2.2.6)		Temperature intervals (K)
Raman mode	Γ_o' (cm^{-1})	A' (cm^{-1})	Γ_0 (cm^{-1})	A (cm^{-1})	
A_1(TO1)	28.0	82.0	27.3	31.3	0 < T < 200.0
	37.6	39.8	32.3	26.6	200.0 < T < 400.0
	107.9	− 142.6	72.2	− 5.5	400.0 < T < 650.0
A_1(TO2)	27.8	165.6	28.6	25.0	0 < T < 200.0
	26.6	406.2	23.4	85.1	200.0 < T < 400.0
	355.7	− 5251.8	25.7	133.0	400.0 < T < 650.0
B_1	59.3	− 92.7	67.7	− 69.1	0 < T < 200.0
	50.1	220.0	37.1	101.7	200.0 < T < 400.0
	69.9	2115.9	70.0	70.6	400.0 < T < 650.0
E(TO1)	11.9	26.6	11.5	16.0	0 < T < 200.0
	49.2	2.9	59.1	− 2.8	200.0 < T < 400.0
	51.8	18.3	51.1	12.3	400.0 < T < 650.0
E(TO2)	25.2	25.3	25.1	7.0	0 < T < 200.0
	146.1	− 1974.1	7.1	117.5	200.0 < T < 400.0
	91.5	− 5452.2	6.4	394.5	400.0 < T < 650.0

Calculations and results

The unit cell volume of PZT ($x = 0.48$) ceramic was calculated by using the empirical formula $V = (abc)sin\beta$, for the monoclinic phase, and $V = a^2c$, for the tetragonal phase, where a, b, and c are the lattice parameters of the unit cell and β is the angle between a and c. This calculation of the unit cell volume performed by using the lattice parameters of this ceramic reported in the literature [15]. The temperature dependence of the unit cell volume is given in Fig. 1. These calculated values of the unit cell volume were then analyzed according to

$$V = d_0 + d_1 T, \tag{3.1}$$

where $d_0$and d_1 are the constants with appropriate units, as given in Table 1 for the temperature intervals indicated. The observed [42] wavenumbers (spatial frequency) of the A_1(TO1), A_1(TO2), B_1, E(TO1), and E(TO2) Raman modes in PZT ($x = 0.48$) ceramic were also analyzed as a function of temperature according to a quadratic equations

$$\omega(T) = e_0 + e_1 T + e_2 T^2, \tag{3.2}$$

here, e_0, e_1, and e_2 are constants with appropriate units as also given in Table 2. Those extracted values of the fitting parameters $d_0$and d_1 of Eq. (3.1) also e_0, e_1, and e_2 of Eq. (3.2) were then used to compute the isobaric mode Grüneisen parameter $\gamma_P(T)$ of the Raman modes in PZT ($x = 0.48$) ceramic, indicated above according to Eq. (2.1.2), as given in Fig. 2. The wavenumbers of the Raman modes in PZT ($x = 0.48$) ceramic were then calculated according to Eq. (2.1.3) by using the values of the $\gamma_P(T)$ (Fig. 2) of the relevant modes in this ceramic. A fitting procedure then performed between the observed [42] and calculated (Eq. 2.1.3) values of the wavenumbers according to

$$\omega_{obs.} = f_0 + f_1\omega_{cal.} + f_2(\omega_{cal.})^2, \tag{3.3}$$

where the constants f_0, f_1, and f_2 are tabulated in Table 3. Figure 3 shows the observed [42] and calculated (Eq. 3.3) values of the wavenumbers as a function of temperature.

Regarding the computation of the damping constant for the Raman modes in PZT ($x = 0.48$) ceramic studied here from the pseudospin-phonon coupled model (Eq. 2.2.4) and from the energy fluctuation model (Eq. 2.2.6), the calculated values of the wavenumbers ω were associated with order parameter according to

$$y = \frac{\omega}{\omega_{max}}, \tag{3.4}$$

since the order parameter y can take any value between 0 and 1. In the last expression, ω_{max} is the maximum value of the wavenumber of the relevant Raman mode. Those calculated values of the damping constant from the two models (Eqs. 2.2.4 and 2.2.6) with help of Eq. (3.4) were then fitted to the observed [37] damping constant data to extract the values of the background damping constant Γ_o' (Γ_0) and the amplitudes A'(A), as given in Table 4 for the temperature intervals indicated. Figure 4 shows the calculated (Eqs. 2.2.4 and 2.2.6) values of the damping constant from both models. The observed [42] data were also given for comparison.

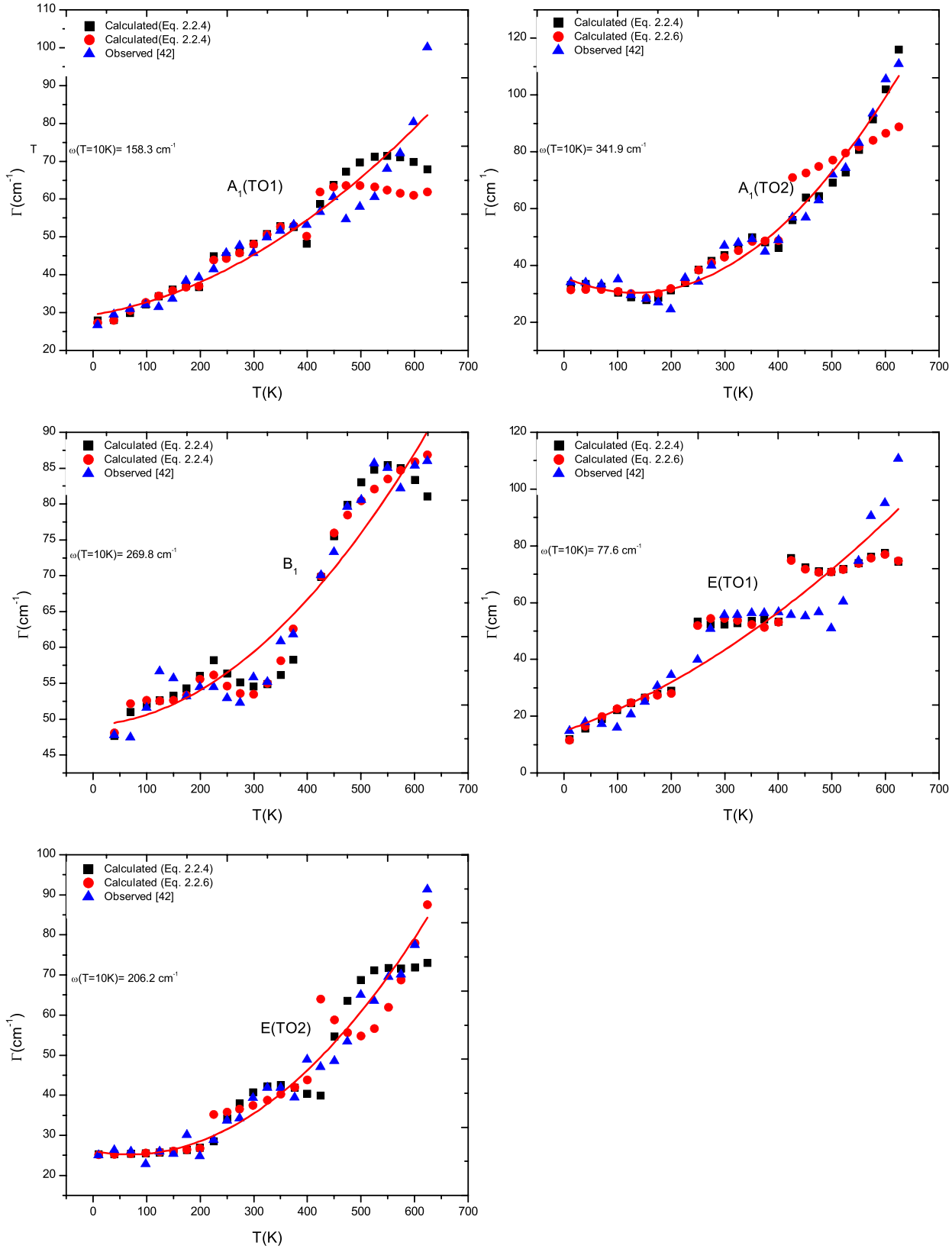

Fig. 4 Damping constant calculated as a function of temperature using the pseudospin-phonon coupled and the energy fluctuation models according to Eqs. (2.2.4) and (2.2.6), respectively, for the Raman modes indicated in PZT ($x = 0.48$) ceramic. The red lines show best fit of Eq. (2.2.10) for the observed [42] damping constant data of these modes

Table 5 Values of the activation energy U and the constant C extracted from Eq. (2.2.8) for the Raman modes indicated in PZT ($x = 0.48$) ceramic by using the pseudospin-phonon coupled Eq. (2.2.4) and the energy fluctuation (2.2.6) models

Raman mode	Damping model	U (meV)	C (cm^{-1})	Temperature intervals (K)	k_BT_C (meV)
A_1(TO1)	Eq. (2.2.4)	16.6	98.5	400.0 < T < 650.0	56.0
	Eq. (2.2.6)	2.6	58.9		
A_1(TO2)	Eq. (2.2.4)	78.5	450.0	400.0 < T < 650.0	
	Eq. (2.2.6)	21.4	134.9		
B_1	Eq. (2.2.4)	17.6	119.9	400.0 < T < 650.0	
	Eq. (2.2.6)	22.5	133.6		
E(TO1)	Eq. (2.2.4)	4.3	81.2	400.0 < T < 650.0	
	Eq. (2.2.6)	5.0	82.6		
E(TO2)	Eq. (2.2.4)	57.6	233.2	400.0 < T < 650.0	
	Eq. (2.2.6)	36.7	145.3		

The k_BT_C value of PZT ($x = 0.48$) ceramic is also given for comparison

The values of the activation energy U were deduced through Eq. (2.2.9) close to the tetragonal-cubic phase transition temperature of $T_C = 650$ K, as tabulated in Table 5. This calculation was performed by using the Γ values calculated from pseudospin-phonon coupled model (Eq. 2.2.4) and from the energy fluctuation model (Eq. 2.2.6). Also, the inverse relaxation time τ^{-1} was predicted as function of temperature through Eq. (2.2.9) for the Raman modes indicated in PZT ($x = 0.48$) ceramic, as given in Fig. 5.

As an extension of this work, the observed data [42] of the damping constant and the wavenumber for the Raman modes in PZT ($x = 0.48$) studied were analyzed by means of the Balkanski model [41] according to Eqs. (2.2.10) and (2.2.11), respectively. The fitting parameters $\Gamma(0)$, $\omega(0)$, A, B, C, and D of these equations are given in Table 6. The characteristic frequency ω_0 of each mode, which was extracted through the extrapolating procedure of the observed [42] wavenumber between $0 < T(K) < 200$ according to Eq. (3.2), is also presented in Table 6.

Finally, the temperature dependence of the unit cell volume of this ceramic (Fig. 1) was used to compute the thermal expansion α_P according to Eq. (2.3.1). In addition, the isothermal compressibility κ_T and the specific heat $C_P - C_V$ were calculated according to Eqs. (2.3.2) and (2.3.3), respectively. For this calculation of κ_T and $C_P - C_V$, the slope of the observed [12] P-T diagram (dP/dT) that is − 0.0147 Gpa/K was used. Figure 6 represents predicted values of the thermal expansion α_P, the isothermal compressibility κ_T, and the specific heat $C_P - C_V$, as a function of temperature for the PZT ($x = 0.48$) ceramic.

Discussion

The volume of the unit cell for PZT for PZT ($x = 0.48$) ceramic calculated in terms of the lattice parameters [15] was doubled below 200 K (Fig. 1), which was an indication of the structural phase transition around 200 K from tetragonal to monoclinic, as also pointed out previously [15]. Equation (2.1.2) was used to

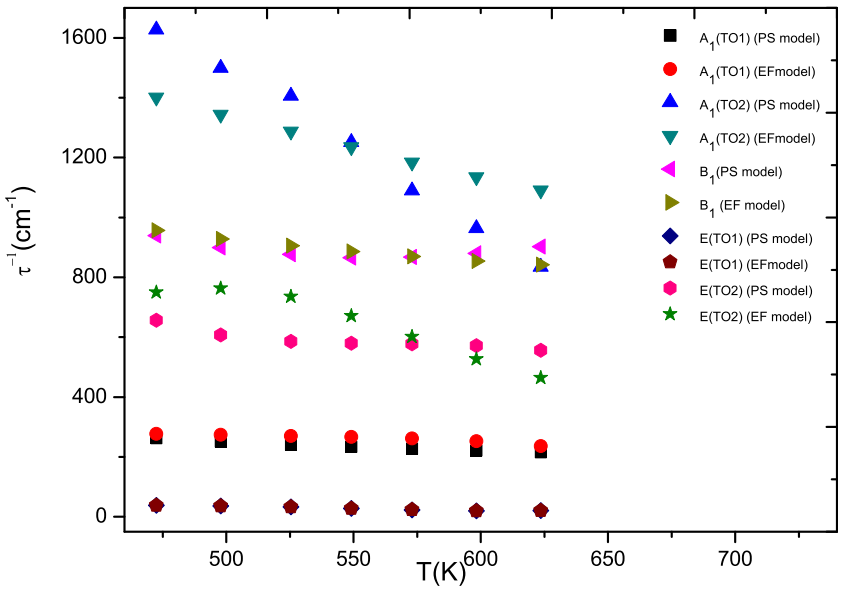

Fig. 5 Inverse relaxation time calculated as a function of temperature using the pseudospin-phonon coupled (PS) and the energy fluctuation (EF) models according to Eq. (2.2.9) for the Raman modes indicated in PZT ($x = 0.48$) ceramic

Table 6 Values of the fitting parameters of Eqs. (2.2.10) and (2.2.11) for the observed [42] Raman modes in PZT ($x = 0.48$) ceramic

Raman mode	$\Gamma(0)$ (cm^{-1})	$Ax10^{-2}$ (cm^{-1})	$Bx10^{-3}$ (cm^{-1})	$\omega(0)$ (cm^{-1})	$-Cx10^{-2}$ (cm^{-1})	$-Dx10^{-4}$ (cm^{-1})	a (K)	ω_0 (cm^{-1})
A_1(TO1)	29.6	17.8	5.3	164.7	60.0	2.27	18.3	159.8
A_1(TO2)	37.8	− 194.5	76.0	343.1	− 0.8	205.0	39.0	340.6
B_1	49.1	1.0	15.2	–	–	–	30.9	270.3
E(TO1)	14.6	31.1	1.1	80.0	29.0	0.2	9.1	79.6
E(TO2)	26.2	− 31.4	15.8	207.4	46.9	46.8	23.6	205.8

The characteristic values of the wavenumber (ω_0) for the observed [42] Raman modes are also given

compute values of the isobaric mode Grüneisen parameters $\gamma_P(T)$ of the A_1(TO1), A_1(TO2), B_1, E(TO1), and E(TO2) Raman modes in PZT ($x = 0.48$) ceramic by using the coefficients of Eq. (3.1) (Table 1) and Eq. (3.2) (Table 2), as given in Fig. 2. It is reported that [43] the Grüneisen parameter values for the soft ferroelectric transverse optic (TO) mode systems ($KTaO_3$, PZTs) were very huge near the transition temperature, as also found in this study for the TO's Raman modes in this PZT ceramic studied here. Especially, the $\gamma_P(T)$ values for the E(TO1) Raman mode in PZT ($x = 0.48$) ceramic increased up to a thousand (1014) close to the ferroelectric-paraelectric transition temperature of 650 K. This is due to the fact that, when the interatomic distances decrease close to the phase transition temperature, the Columb forces increase much more slowly than do the short-range forces which causes a large change in phonon frequency with a small variation in crystal volume according to Eq. (2.1.1). Those calculated values of the $\gamma_P(T)$ values were used to evaluate the temperature dependence of the wavenumbers of the Raman modes in PZT ($x = 0.48$) ceramic studied according Eq. (2.1.3), as given in Fig. 3. This figure showed the harmony between the calculated (Eqs. 2.1.3 and 3.3) and the observed [37] data for the wavenumbers of the Raman modes studied here.

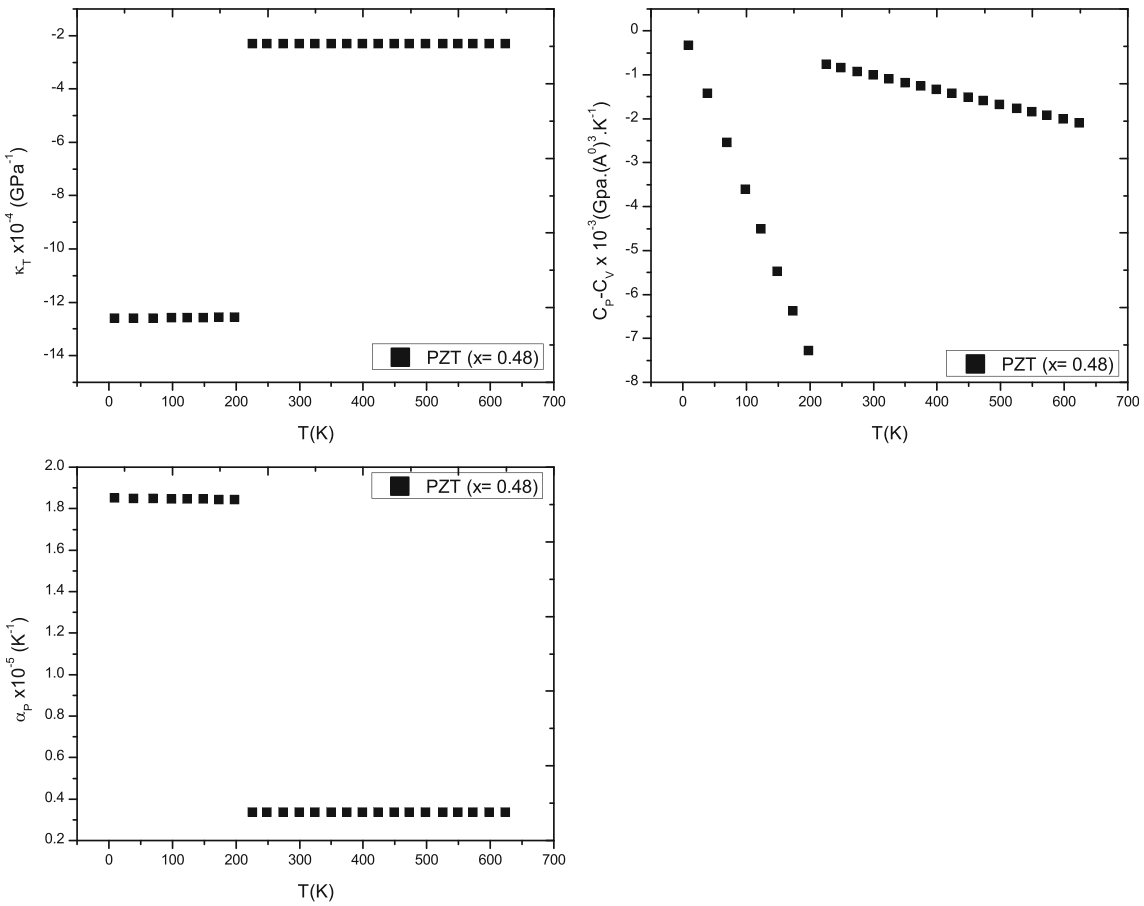

Fig. 6 Temperature dependence of the thermal expansion α_P (Eq. 2.3.1), isothermal compressibility κ_T (Eq. 2.3.2), and the specific heat $C_P - C_V$ (Eq. 2.3.3) from the observed [12] P-T data of PZT ($x = 0.48$) ceramic

The damping constant (linewidth) of the Raman modes in PZT ($x = 0.48$) ceramic studied was also calculated from the pseudospin-phonon coupled (Eq. 2.2.4) and the energy fluctuation (Eq. 2.2.6) models, as given in Fig. 4. This figure shows the consistency of the temperature-dependent damping constant between the observed [42] and calculated (Eqs. 2.2.4 and 2.2.6) data for the Raman modes studied here except the E_1(TO1) mode between 400 and 650 K and also for the A_1(TO1) mode between 550 and 650 K. The damping constant increases as the temperature increases as also observed [42] experimentally up to the transition temperature of 650 K from tetragonal to cubic phase. In our earlier works, we used these two models to describe the phase transition mechanism of some ferroelectric materials such as $BaTiO_3$ [44], KH_2PO_4 [45], $PbTiO_3$ [46], $SrZrO_3$ [47], $(NH_4)_2SO_4$ [48], and $SrTiO_3$ [49].

The extracted values of the activation energy U for the PZT ($x = 0.48$) ceramic through Eq. (2.2.8) in terms of the damping constant calculated from both pseudospin-phonon coupled and the energy fluctuation models are tabulated in Table 5. The varied U values between 2.6 and 78.5 meV can be compared with the $k_B T_C$ value of 56.0 meV, as also given in Table 5. This indicates that both models studied are adequate to describe the observed behavior of the linewidths of the Raman modes in the ferroelectric phase of PZT ($X = 0.48$) ceramic. The inverse relaxation time τ^{-1} of the Raman modes studied was predicted according to Eq. (2.2.9) in terms of the calculated Γ (Fig. 4) and ω (Fig. 2) values close to the transition temperature $T_C = 650$ K. τ^{-1} decreased as the temperature increased up to the T_C, as given in Fig. 5. Although no experimental data were found for the $\tau^{-1}$of PZT ($x = 0.48$) ceramic to compare with, those calculated values of τ^{-1} can be compared with the observed [8] data of PZT ($x = 0.45$) single crystal which shows similar gradually decreasing behavior as the temperature increases in the ferroelectric phase ($T < T_C$) of this single crystal ($T_C = 657$ K).

With regard the anharmonic effects in lattice vibrations, the analysis of the observed damping constant and the wavenumber data [42] of these studied Raman modes in PZT ($x = 0.48$) according to Eqs. (2.2.10) and (2.2.11) fit well, with the fitting parameters given in Table 6 except one mode, as also shown in Figs. 3 and 4. Although the damping constant data of B_1 mode converged according to Eq. (2.2.10), the wavenumber data did not. Unlike the observed wavenumber data, which are almost constant with increasing temperature T, it is reported that [41] in the high-temperature limit, the fitting parameters C and D of Eq. (2.2.11) vary as T and T^2, respectively. On the other hand, the extracted values of the $\Gamma(0)$ for the Raman modes studied (Table 6) are very close to those values of the background damping constant Γ_o and Γ_0 calculated from the pseudospin-phonon coupled (Eq. 2.2.4) and the energy fluctuation (Eq. 2.2.6) models in the temperature interval of $0 < T(K) < 200$ (Table 4).

Figure 6 shows the values of the volume thermal expansion α_P, the isothermal compressibility κ_T, and the specific heat $C_P - C_V$ of PZT ($x = 0.48$) ceramic as a function of temperature predicted through Eqs. (2.3.1, 2.3.2, and 2.3.3), respectively. The anomalous behaviors of α_P, κ_T, and $C_P - C_V$ around 200 K were an indication of the structural phase transition from monoclinic to tetragonal phase. The $C_P - C_V$ decreases rapidly as the temperature increased from 0 to 200 K, while it decreases more slowly as temperature increased from 200 K up to the phase transition temperature of 650 K. The step-like behaviors of α_P and κ_T (Fig. 6) indicated that the thermodynamic quantities were weakly temperature dependent below and above the phase transition temperature of 200 K.

Conclusions

The spectroscopic quantity wavenumber of some Raman modes in PZT ($x = 0.48$) ceramic was calculated as a function of temperature through the simple microscopic definition of the Grüneisen parameter that was also computed in this study. The damping constant of the Raman modes studied was also calculated from the psedospin-phonon coupled and the energy fluctuations models. In addition, those calculated values of the wavenumber and the damping constant for the Raman modes in PZT ($x = 0.48$) ceramic studied were also detailed in view of the Balkanski model in order to compare with a recognized theory of anharmonic effects in lattice vibrations. The psedospin-phonon coupled and the energy fluctuations models may contribute to explain the complex order-disorder phase transition mechanism of some other ferroelectric ceramics. Additionally, temperature dependence of the inverse relaxation time was predicted, and also, the values of the activation energy of this ceramic were computed. The predicted values of the thermodynamic quantities, thermal expansion, isothermal compressibility, and the specific heat for PZT ($x = 0.48$) ceramic can be compared with the experimental data when they are available in the literature.

References

1. Uchino, K.: Piezoelectric ultrasonic motors: Overview. Smart Mater Struct. **7**, 273–285 (1998)
2. Moulson, A.J., Herbert, J.M.: Electroceramics: Materials, Properties and Applications, first edn. Chapman and Hall, London (1990)

3. Jaffe, B., Cook Jr., W.R., Jaffe, H.: Piezoelectric Ceramics, first edn. Academic Press, London (1971)
4. Michel, C., Moreau, J.-M., Achenbach, G.D., Gerson, R., James, W.J.: Atomic structures of two rhombohedral ferroelectric phases in the $Pb(Zr,Ti)O_3$ solid solution series. Solid State Commun. **7**, 865–868 (1968)
5. Glazer, A.M., Mabud, S.A., Clarke, R.: Powder profile refinement of lead zirconate titanate at several temperatures. I. $PbZr_{0.9}$ $Ti_{0.1}O_3$. Acta Crystallograph B. **34**, 1060–1065 (1978)
6. Cereceda, N., Noheda, B., Gonzalo, J.A., Mielcarek, S., Mroz, B.: Specific heat, charge release and dielectric constant of PZT ceramics. J Korean Phys Soc. **32**, 241–243 (1998)
7. Shirane, G., Takeda, A.: Phase transitions in solid solutions of $PbZrO_3$ and $PbTiO_3$ (I) small concentrations of $PbTiO_3$. J Phys Soc Jpn. **7**, 5–11 (1952)
8. Kim, T.H., Ko, J.-H., Kojima, S., Bokov, A.A., Long, X., Ye, Z.-G.: Phase transition behaviors of $PbZr_{1-x}Ti_x$ O_3 single crystals as revealed by elastic anomalies and central peaks. Appl Phys Lett. **100**, 082903–082908 (2012)
9. Bouzid, A., Bourim, E.M., Gabbay, M., Fantozzi, G.: PZT phase diagram determination by measurement of elastic moduli. J Eur Ceram Soc. **25**, 3213–3221 (2005)
10. Eitel, R., Randall, C.A.: Octahedral tilt-suppression of ferroelectric domain wall dynamics and the associated piezoelectric activity in $Pb(Zr,Ti)O_3$. Phys Rev B. **75**, 094106–094113 (2007)
11. Buixaderas, E., Nuzhnyy, D., Petzelt, J., Jin, L., Damjanovic, D.: Polar lattice vibrations and phase transition dynamics in $Pb(Zr_{1-x}Ti_x)O_3$. Phys Rev B. **84**, 184302–184313 (2011)
12. Rouquette, J., Haines, J., Bornand, V., Pintard, M., Papet, P., Bennet, B., Gorelli, F.A.: P-T phase diagram of $PbZr_{0.52}Ti_{0.48}$ O_3 (PZT). Sol. Stat Sci. **5**, 451–457 (2003)
13. Audigier, D., Richard, C., Deschamps, C., Troccaz, M., Eyraud, L.: PZT uniaxial stress dependence: experimental results. Ferroelectrics. **154**, 219–224 (1994)
14. Cho, K.H., Seo, C.E., Choi, Y.S., Ko, Y.H., Kim, K.J.: Effect of pressure on electric generation of PZT(30/70) and PZT(52/48) ceramics near phase transition pressure. J Eur Ceram Soc. **32**, 457–463 (2012)
15. Noheda, B., Cox, D.E., Shirane, G., Gonzalo, J.A., Cross, L.E., Park, S.-E.: A monoclinic ferroelectric phase in the $Pb(Zr_{1-x}Ti_x)O_3$ solid solution. Appl Phys Lett. **74**, 2059–2061 (1999)
16. Phelan, D., Long, X., Xie, Y., Ye, Z.-G., Glazer, A.M., Yokota, H., Thomas, P.A., Gehring, P.M.: Single crystal study of competing rhombohedral and monoclinic order in lead zirconate titanate. Phys Rev Lett. **105**, 207601–207605 (2010)
17. Hlinka, J., Ondrejkovic, P., Kempa, M., Borissenko, E., Krisch, M., Long, X., Ye, Z.-G.: Soft antiferroelectric fluctuations in morphotropic $PbZr_{1-x}Ti_xO_3$ single crystals as evidenced by inelastic X-ray scattering. Phys Rev B. **83**, 140101–140103 (2011)
18. Gorfman, S., Keeble, D.S., Glazer, A.M., Long, X., Xie, Y., Ye, Z.-G., Collins, S., Thomas, P.A.: High-resolution X-ray diffraction study of single crystals of lead zirconate titanate. Phys Rev B. **84**, 020102–020105 (2011)
19. Bokov, A.A., Long, X., Ye, Z.-G.: Optically isotropic and monoclinic ferroelectric phases in $Pb(Zr_{1-x}Ti_x)O_3$ (PZT) single crystals near morphotropic phase boundary. Phys Rev B. **81**, 172103–172106 (2010)
20. Filho, A.G.S., Faria, J.L.B., Freire, P.T.C., Ayala, A.P., Sasaki, J.M., Melo, F.E.A., Filho, J.M., Arau´jo, E.B., Eiras, J.A.: Monoclinic phase of $PbZr_{0.52}Ti_{0.48}$ O_3 ceramics: Raman and phenomenological thermodynamic studies. Phys Rev B. **61**, 14283–14286 (2000)
21. Rouquette, J., Haines, J., Bornand, V., Pintard, M., Papet, P., Astier, R., Léger, J.M., Gorelli, F.: Transition to a cubic phase with symmetry-breaking disorder in $PbZr_{0.52}Ti_{0.48}$ O_3 at high pressure. Phys Rev B. **65**, 214102 (2002)
22. Yokota, H., Zhang, N., Taylor, A.E., Thomas, P.A., Glazer, A.M.: Crystal structure of the rhombohedral phase of $PbZr_{1-x}Ti_xO_3$ ceramics at room temperature. Phys Rev B. **80**, 104109 (2009)
23. Corker, D.L., Glazer, A.M., Whatmore, R.W., Stallard, A., Fauth, F.J.: A neutron diffraction investigation into the rhombohedral phases of the perovskite series $PbZr_{1-x}Ti_xO_3$. J Phys Condens Matter. **10**, 6251–6269 (1998)
24. Frantti, J., Ivanov, S., Lappalainen, J., Eriksson, S., Lantto, V., Nishio, S., Kakihana, K., Rudlöf, H.: Local and average structure of lead titanate based ceramics. Ferroelectrics. **266**, 73–90 (2002)
25. George, A.M., Íñiguez, J., Bellaiche, L.: Optical phonons associated with the low-temperature ferroelectric properties of perovskite solid solutions. Phys Rev B. **65**, 180301 (2002)
26. Grinberg, I., Cooper, V.R., Rappe, A.M.: Relationship between local structure and phase transitions of a disordered solid solution. Nature (London). **419**, 909–911 (2002)
27. Hlinka, J., Petzelt, J., Kamba, S., Nouijini, D., Ostapchuk, T.: Infrared dielectric response of relaxor ferroelectrics. Phys Transit. **79**, 41–78 (2006)
28. yurtseven, H., Kiraci, A.: Damping constant (linewidth) and the relaxation time of the brillouin LA mode for the ferroelectric-paraelectric transition in $PbZr_{1-x}Ti_xO_3$. IEEE Trans Ultrason Ferroelectr Freq Control. **63**, 1647–1655 (2016)
29. Gruneisen, E.: Theorie das fasten zustandes einatomiger elemente. Ann Phys. **12**, 257–306 (1912)
30. Anderson, D.L.: Theory of the Earth. Blackwell scientific publication, Oxford (1989)
31. Yamada, Y., Mori, M., Noda, Y.A.: Microscopic theory on the phase transitions in NH4Br –an Ising spin phonon coupled system. J Phys Soc Jpn. **32**, 1565–1576 (1972)
32. Matsushita, M.: Anomalous temperature dependence of the frequency and damping constant of phonons near T_λ in ammonium halides. J Chem Phys. **65**, 23–28 (1976)
33. Laulicht, I., Luknar, N.: Internal-mode line-broadening by proton jumps in KH_2PO_4. Chem Phys Lett. **47**, 237–240 (1977)
34. Laulicht, I.: On the drastic temperature broadening of hard mode Raman lines of ferroelectric KDP type crystals near T_c. J Phys Chem Solids. **39**, 901–906 (1978)
35. Lahajnar, G., Blinc, R., Zumer, S.: Proton spin-lattice relaxation by critical polarization fluctuations in KH_2PO_4. Phys Cond Matter. **18**, 301–316 (1974)
36. Schaack, G., Winterfeldt, V.: Temperature behaviour of optical phonons near T_c in triglycine sulphate and triglycine selenate. Ferroelectrics. **15**, 35–41 (1977)
37. Rakov, A.V.: The influence of the intermolecular interaction on line width in the Raman spectra of liquids. Opt Spectrosc. **7**, 128–134 (1959)
38. Bartoli, F.J., Litovitz, T.A.: Raman scattering: orientational motions in liquids. J Chem Phys. **56**, 413–425 (1972)
39. Fahim, M.A.: A detailed IR study of the order–disorder phase transition of $NaNO_2$. Thermochim Acta. **363**, 121–127 (2000)
40. Hart, T.R., Aggarwal, R.L., Lax, B.: Temperature dependence of raman scattering in silicon. Phys Rev B. **1**, 638–642 (1970)
41. Balkanski, M., Wallis, R.F., Haro, E.: Anharmonic effects in light scattering due to optical phonons in silicon. Phys Rev B. **28**, 1928–1934 (1983)
42. Buixaderas, E., Bovtun, V., Kempa, M., Nuzhnyy, D., Savinov, M., Vanek, P., Gregora, I., Malic, B.: Lattice dynamics and domain wall oscillations of morphotropic $Pb(Zr,Ti)O_3$ ceramics. Phys Rev B. **94**, 054315 (2016)
43. Samara, G.A.: The grüniesen parameter of the softferroelectric mode in the cubic perovskites. Ferroelectrics. **2**, 177–182 (1971)
44. Kiraci, A., Yurtseven, H.: Damping constant calculated as a function of temperature for the tetragonal Raman mode close to the Paraelectric-ferroelectric transition in $BaTiO_3$. Ferroelectrics. **450**, 93–98 (2013)

45. Karacali, H., Kiraci, A., Yurtseven, H.: Calculation of the Raman frequency and the damping constant of a coupled mode in the ferroelectric and paraelectric phases in KH_2 PO_4. Phys Status Solidi B. **247**, 927–936 (2010)
46. Kiraci A., Yurtseven H. Calculation of the damping constant and the order parameter for the lattice mode in ferroelectric $PbTiO_3$, IEEE International Symposium on the Applications of Ferroelectric and Workshop on the Piezoresponse Force Microscopy (ISAF/PFM), (2013) 53–55
47. Yurtseven, H., Kiraci, A.: Temperature dependence of the damping constant and the relaxation time close to the tetragonal-cubic phase transition in $SrZrO_3$. J Mol Struct. **1128**, 51–56 (2017)
48. Yurtseven, H., Karacali, H., Kiraci, A.: Calculation of the damping constant and activation energy for raman modes in $(NH4)_2SO4$. Int J Mod Phys B. **25**, 2063–2080 (2011)
49. Kiraci, A., Yurtseven, H.: Pressure-dependent Raman modes near the cubic-tetragonal transition in strontium titanate. J Am Ceram Soc. **101**, 1344–1355 (2018)